RAL-TR-2006-005

A MONTE CARLO STUDY OF THE PERFORMANCE OF A 1-D IMAGING GAS MICROSTRIP DETECTOR FOR THE CRISP BEAMLINE ON ISIS

J.E.Bateman, D.M.Duxbury, N.J.Rhodes, E.M.Schooneveld and R.Stephenson

Rutherford Appleton Laboratory, Chilton, Didcot, Oxon, OX11 0QX, U.K.

13th June 2006

Abstract

A Monte Carlo model has been developed to simulate the interaction of a slow neutron beam with a ^{3}He filled gas microstrip detector (MSGC). The model permits the exploration of the trade off between the spatial resolution and neutron detection efficiency of the design proposed for neutron reflectometry experiments on the CRISP beamline on ISIS.

1. Introduction

Following the successful testing of a 2D imaging detector based on the gas microstrip detector (GMSD, MSGC) technology [1,2] on the ROTAX beamline at ISIS, it became clear that this technology could offer significant detection capabilities for further experiments on ISIS beamlines. Based on a ^{3}He neutron converter with added quencher, this technology can offer a high rate capability with good timing resolution combined with a low gamma sensitivity and sub millimetre spatial resolution. The inevitable trade off between neutron detection efficiency and spatial resolution, is set by the counter depth, the gas pressure and the electronic discriminator threshold. This trade off is largely determined by the range of the reaction products from the ^{3}He-neutron reaction (a proton and a triton) which can conveniently be examined by the use of a Monte Carlo model of the interaction of these particles with the gas. A similar study has previously been undertaken [3] and the work reported here is based extensively on the model used in reference 3.

As is reported in [4] the MC approach to modelling detectors is seen as a partial replacement for the more traditional role of making a prototype detector in the design process, which is becoming less economically viable. Some of the detector requirements for the proposed detector for CRISP, which would have traditionally been explored with a prototype are:

i. achieving a position resolution of 0.5mm or better (FWHM)
ii. neutron detection efficiency $\geq$ 50% @ 1 Å
iii. readout pitch of 0.5mm minimum

The simulations focus on these parameters. A further requirement is the minimisation of the active length of the detector in order to reduce parallax and neutron flight time errors.

2. The Monte Carlo model

The basis of the model has been adequately described in [3] and will only be briefly described here. The model was used to evaluate the design parameters of the following four applications:

i. a high spatial resolution (<0.5mm), low efficiency beam monitor;
ii. an imaging detector with ~1mm spatial resolution and intermediate detection efficiency for the study of engineering samples;
iii. a gas pixel detector for neutron diffraction studies;
iv. an evaluation of the performance of a very high pressure MSGC.

The model accurately described the experimental results obtained for the MSGC based beam monitor [5], for the imaging 2D prototype MSGC data [1,2] and for the

pin pixel detector [6]. The code has since been modified to simulate a different geometry and also to include the effects of diffusion. These modifications are described in more detail below.

In its basic form the model generates randomly orientated, back to back paths for the recoil proton (570keV) and triton (200keV) within a cell of the MSGC. The paths of these particles are traced until they either stop in a cell or until they pass out of the detector volume. The energy deposit in each cell traversed is evaluated and stored in an array using the range energy data published in [7]. A separate array sums all cell hits which are defined when the energy deposit in a cell exceeds the pre-set electronic lower level discriminator threshold (LLD) which is defined in terms of the equivalent energy deposit in units of MeV.

For each run of the simulation, 10^4 starts are made on the basic loop, which corresponds to that number of neutrons interacting within the gas. The conversion efficiency is simply calculated from the total stopping power of the ^{3}He multiplied by the cross section at a neutron wavelength of 1Å. It should be noted that all the results presented here are for a neutron wavelength of 1Å unless otherwise stated. The readout efficiency is measured as the fraction of 'starts' which result in at least one hit in a cell above the lower level threshold. The detection efficiency is thus the product of the readout efficiency and the conversion efficiency. Often there is more than one hit per interacting neutron. The multiplicity is defined as the area of the cell count profile divided by the number of starts.

Unless otherwise stated, the model simulates the point spread function (PSF) of the detector, which is the response of the system to an input delta function. The incident 'neutrons' are all generated at the centre of the zero pixel, but are allowed to interact throughout its depth as would be the case for real neutrons.

In order to include the effects of diffusion, each secondary electron distribution created in the gas is convolved with a Gaussian spreading variable, which is dependent on the diffusion constant, σ_o, for the gas mixture. (σ_o [$\mu m/\sqrt{cm}$] is the standard deviation of the Normal distribution of a quasi-punctual source resulting from diffusive drift over a distance of 1cm.) Ideally we would track every electron in the distribution (~28000) but this is time consuming in terms of computing time. In order to reduce this time, the concept of the 'pseudo electron' was introduced. The average energy to produce an electron ion pair (w_{ei}) in the gas is 27eV. If we increase this energy to 270eV or 2700eV we can run the simulation much quicker, providing that the results are not adversely effected. Figure 1 shows a hit distribution comparing the three values of w_{ei}. By comparing a Gaussian fit to each of these distributions we can see that the width of the distribution (sigma) is marginally increased by increasing w_{ei}. By choosing a value of w_{ei} equal to 270eV we will very slightly over estimate sigma but dramatically reduce the computing time. Each pseudo electron is represented on the detector plane as a sample of the Normal distribution resulting from the diffusion spreading induced by the drift length and diffusion constant.

Provision is made for an arbitrary choice of detector geometry i.e. the depth (d) (along the beam), the width (or pitch) (c) and the height (h) of the detector cells. Similarly an arbitrary mixture of helium and quencher may be specified with the appropriate density and atomic number for the quencher used. It should be clarified

here that there is no ‘stopping gas’ as there is in other gas based neutron detectors (for example Argon). The quencher of choice (in this case CF_4) is both the quencher and the stopping gas. To first order the neutrons are only absorbed by the ^{3}He so the quencher can be ignored for the purpose of calculating the efficiency. Conversely, the quencher is much denser than the ^{3}He, thus for the purpose of localising the reaction products the ^{3}He can be neglected. The span of the cells required to contain the events under any given specification is self adjusting.

The model was used to simulate two different MSGC geometries. A conventional ‘face-on’ MSGC (where the drift of the electrons is in a parallel direction to that of the neutron beam), and a ‘pointing-anode’ geometry [8,9] (where the drift of electrons is in an orthogonal direction to the neutron beam). In the latter case, the parameter d now just sets the drift depth and the parameter h (the length of the active strip) will now determine the neutron interaction depth, along which the neutron detection efficiency is calculated.

3. A One dimensional detector for CRISP

The CRISP reflectometer on ISIS [10,11] is a station which is primarily used for time of flight neutron reflection experiments from surfaces and interfaces. This powerful technique can also be used on CRISP to look at liquid surfaces. In its specular reflection mode the instrument uses a single, one inch diameter ^{3}He detector filled with 10 bars of ^{3}He [12] and the sample to detector distance is 1.87m. To measure off specular reflectivity the single ^{3}He detector is replaced either with a linear position sensitive Ordela 1202N ^{3}He wire detector [13] or a fibre coded ZnS:Ag/^{6}LiF scintillation detector [14]. The Ordela detector is rise time encoded and suffers from dead time and is easily damaged by the straight through beam of neutrons. The scintillation detector has a higher rate capability and is more robust, but is limited to a position resolution of 1.2mm. Improving the detector resolution and the count rate performance will enable the reflected and non-reflected spectra to be probed in more detail. In order to implement these changes we propose to build a system based on the gas microstrip detector with the following performance specification:

- a position resolution of 0.5mm or better (FWHM)
- a neutron detection efficiency $\geq$ 50% @ 1 Å
- an active area of 320mm by preferably 80mm (minimum 50mm)
- a readout pitch of 0.5mm minimum (giving us 640 electronic readout channels)
- a local count rate performance of at least 10^5 counts per second
- a dynamic range of 6 orders of magnitude
- a count rate stability of 0.5% per 48 hours

- a gamma sensitivity of 10^{-8} at 1.3MeV

- a detector background of <10 counts per hour over the whole active area.

The sample to detector distance of 1.87m on CRISP poses a potential parallax problem. Initial simulations showed (figures 2 and 3) that if we wanted to achieve a high neutron detection efficiency, then we would either need to pressurise a vessel to around 10 bars of ^{3}He and have a thin gas depth, or we would need a large absorption depth (say 50mm) and only a few bars of ^{3}He. However, with a 50mm gas depth, at 1.87m, we would have a parallax error of 4.3mm! A similar problem was encountered with an x-ray detector which was developed at RAL [8,9] the solution to which was to change the electrode design and geometry of the detector to have electrodes which pointed to the scattering sample position, and to have the x-rays enter the gas volume parallel to these pointing electrodes. With this geometry, the neutron absorption depth is now only limited by the length of the electrodes. An alternative method of reducing the effects of parallax with a face-on geometry, is to utilise some form of field shaping to remove parallax. This has been done on a similar type of detector at the Brookhaven National Laboratory [15]. Both geometries were therefore simulated and a comparison of the two made.

In order to keep the number of simulations to a minimum and to keep the comparison as simple as possible, as many parameters that could be fixed for both cases were set the same. The readout pitch was fixed to 0.5mm, the drift depth was fixed to 50mm (this is the neutron interaction depth for the case of the face on geometry). The strip length was set to 80 mm for the face-on case and 65mm for the pointing-anode case (this is the interaction depth for the pointing-anode case). This now leaves us with 4 parameters:

i. the electronic lower level discriminator threshold LLD
ii. ^{3}He partial pressure
iii. the quencher partial pressure
iv. and the diffusion constant σ_o

The quencher chosen for the simulations is tetrafluoromethane, CF_4. This is the quencher of choice as it is non-neutron sensitive and has a high density which thus helps reduce the range of the proton and triton. In fact the density of CF_4 is 29 times that of ^{3}He, hence validating the assumption that the quencher does all the localising of the reaction products. CO_2 has previously been used as a quencher [16] but the proton and triton ranges are twice as large compared to CF_4. Figure 3 shows that with a 50mm drift depth, there is no need to increase the ^{3}He pressure above approximately ~5bars in order to achieve the desired neutron efficiency. In order to keep the total gas pressure below 10 bars (for ease of engineering and manufacturing) this means that the pressure of the CF_4 will not go above 5 bars either. The diffusion coefficient parameter σ_o, is varied from 50 to 300 $\mu m/\sqrt{cm}$ as there is very little data available in the scientific literature for our gas mixture of ^{3}He:CF_4. In general σ_o is optimally ~200$\mu m/\sqrt{cm}$ for a hydrocarbon and noble gas mixture [17] as figure 4 shows (adapted from figure 92 in [17]). Increasing the gas pressure tends to make σ_o follow the thermal limit curve for higher values of E/P, as demonstrated by figure 200 in

[17]. As the pressure is increased the curve gets closer and closer to the thermal limit, but the minimum drift field tends to increase. On this basis we expect 150-200μm/√cm to be a plausible value for a 50:50 mixture of ^{3}He:CF_4 at 1 bar pressure, and it may be lower than this at the higher pressures which we intend to operate. The LLD is varied between 0.1 and 0.45MeV.

For the face-on and pointing-anode detector geometries, we can systematically vary the parameters (within our ranges) for comparison. Figure 5 shows a typical distribution for the pointing anode case, with 4 bars of ^{3}He, 4 bars of CF_4, a σ_o of 200μm/√cm and an LLD of 0.35MeV. For these settings we achieve a neutron efficiency of 36.4%. A Gaussian fit to the distribution yields a sigma of 0.194mm, which when multiplied by 2.36 gives us a FWHM resolution of 0.457mm. Figures 6-9 show how the spatial resolution (the sigma from the fit) varies with the detection efficiency as the LLD threshold is changed. Each curve on the graph represents a different value of σ_o as indicated. The four figures represent the four gas mixtures of 3:3; 3.5:3.5; 4:4 and 4.5:4.5 bars of ^{3}He:CF_4 for the case of the face-on geometry. The plots also show the results for the case where we set the simulations to have no electron diffusion. The horizontal line on the plots indicate the value of sigma which gives us a FWHM resolution of 0.5mm. Figures 10-13 show the same data for the case of the pointing-anode style geometry. We can see from the plots, for both the face-on and the pointing-anode case, that as the LLD is increased, the efficiency goes down, as you would expect when more pulses fall below threshold. We also find that sigma is reduced as the LLD is increased, again as would be expected when the smaller pulses are removed thus giving a sharper distribution. By increasing the amount of ^{3}He we get a corresponding increase in the efficiency and by increasing the amount of CF_4 we obtain a reduced value of sigma, again as expected. When the diffusion constant σ_o is increased, we have two separate behaviour patterns which can be seen in figure 14, which shows the 4.5:4.5 bar ^{3}He:CF_4 data for the pointing anode geometry. At an LLD of 0.2MeV and below, the efficiency is reduced and the sigma increases as σ_o increases. But at an LLD of 0.3MeV and above, as σ_o is increased the efficiency is reduced but sigma decreases. In general the resolution figures for the face-on geometry are slightly worse compared to the pointing-anode ones (but not by much). This is shown directly in figure 15 which compares the two geometry's with a 4.5:4.5 gas mixture and with σ_o set to 150μm/√cm. The main difference between the two is that the efficiency is greater in the pointing-anode case, for the same gas mixture by virtue of the extended interaction depth. The fact that one can operate the pointing-anode style detector at half a bar less of each gas, for roughly the same detector performance, combined with the parallax free detection, makes it a much more attractive option for OSMOND, given that we have limited experience of running these detector at such elevated pressures.

The detector readout uniformity, or differential non-linearity (DNL), warrants discussion, as it degrades the imaging performance of the detector and needs to be minimised. Variations in counter gain and electronic component tolerances leading up to the discriminator make it difficult to reduce this intrinsic variation below ~5%. Figure 16 shows the variation of sigma and detection efficiency as the LLD is increased. The graph also shows how the multiplicity varies as the LLD is increased. The multiplicity is defined as the area of the cell count profile divided by the number of starts. The apparent efficiency, which is also plotted on figure 16 is merely the product of the detection efficiency and the multiplicity. A fit to the apparent

efficiency curve (ignoring the point at an LLD of 0.1MeV) yields a linear expression. The gradient of this curve has been defined elsewhere [18] as the differential non-linearity multiplier (DNM). If we denote the apparent readout efficiency by the symbol y and the corresponding LLD setting by x, then DNM = (dy/y)/(dx/x)=(x/y)(dy/dx). In the case shown in figure 16 the gradient of the fit is ~3.9 and evaluating the expression at an LLD of 0.35MeV (corresponding to our required resolution) gives a DNM = (0.35/0.64)*3.9 = 2.13. In other words our DNL is increased to ~11%. Previously, these effects have been minimised experimentally [16,19] by scanning a wide beam across the detector and adjusting the LLD settings and equalising the channel counts. A uniformity of 2-4% has been measured.

4. Conclusions

The Monte Carlo simulations presented above indicate that an MSGC based detector of the pointing anode geometry could meet the detector requirements for the CRISP instrument on ISIS, namely a position resolution of 0.5mm FWHM combined with a high efficiency ≥50% @ 1 Å. These are both achievable at relatively low pressures of ^{3}He due to the large neutron interaction depth and with no parallax for the case of the pointing anode geometry.

Previous experience has shown that these devices can be operated with 2.5 bars ^{3}He and 2.5 bars CF_4. The jump to 3-4 bars of each gas should not prove to be problematic.

A facility development grant has been awarded to develop a sub-millimetre resolution MSGC for neutron reflectometry. The development is for an Off Specular MicrOstrip Neutron Detector (OSMOND) for the CRISP facility, the design of which has adopted the pointing-anode electrode structure simulated in this paper. The mechanical design of the vessel is currently underway.

If the parallax reduction method [15] could successfully be implemented then the face-on geometry could still be a viable option as a high counting rate, high resolution 2D neutron detector.

References

1. J.E. Bateman, G.E. Derbyshire, D.M. Duxbury, A.S. Marsh, N.J. Rhodes, E.M. Schooneveld, E.J. Spill and R. Stephenson, RAL-TR-2004-028

2. J.E. Bateman, G.E. Derbyshire, D.M. Duxbury, A.S. Marsh, N.J. Rhodes, E.M. Schooneveld, E.J. Spill and R. Stephenson, IEEE Trans. Nucl. Sci **52 (5)** (2005) 1693

3. J.E. Bateman, N.J. Rhodes and R. Stephenson, RAL-TR-1998-024

4. J.E. Bateman, RAL-TR-2005-010

5. J.E. Bateman, N.J. Rhodes and R. Stephenson, Nucl. Instr. and Method **A477** (2002) 365

6. J.E.Bateman, J.F.Connolly, G.E.Derbyshire, D.M Duxbury, A.S.Marsh, N.J. Rhodes, E.M.Schooneveld, J.E. Simmons and R.Stephenson, Nucl. Instr. and Method **A485** (2002) 596

7. J F Janni, (1982) Atomic Data and Nuclear Data Tables, 27, Nos 2-5

8. J.E.Bateman, J.F.Connolly, G.E.Derbyshire, A.S.Marsh, R.Stephenson, J.E. Simmons, E.J.Spill, B.R.Dobson, R.C.Farrow, W.I.Helsby, R. Mutikainen and I.Suni, RAL-TR-1998-073

9. J.E.Bateman, J.F.Connolly, G.E.Derbyshire, D.M.Duxbury, J.Lipp, J.A.Mir, J.E. Simmons, E.J.Spill, R.Stephenson, B.R.Dobson, R.C.Farrow, W.I.Helsby, R. Mutikainen and I.Suni, Nucl. Instr. and Method **A477** (2002) 340

10. J. Penfold, R.C. Ward and W.G. Williams, J. Phys. E: Sci. Instrum. **20** (1987) 1411

11. J. Penfold, Physica B **173** (1991) 1

12. http://www.gepower.com/prod_serv/products/radiation_monitors/en/security_safeguards/h3_counter.htm

13. http://www.ordela.com

14. N.J.Rhodes, A.G.Wardle, A.J.Boram and M.W.Johnson, Nucl. Instr. and Method **A392** (1997) 315

15. P. Rehak, G.C. Smith and B.Yu, IEEE Trans. Nucl. Sci **44(3)** (1997) 651

16. J.E. Bateman, N.J. Rhodes and R. Stephenson, RAL-TR-1997-021

17. A.Peisert and F.Sauli, CERN 84-08

18. J.E. Bateman, RAL-TR-2006-004

19. J.E. Bateman, G.E. Derbyshire, D.M. Duxbury, A.S. Marsh, N.J. Rhodes, E.M. Schooneveld, E.J. Spill and R. Stephenson, RAL-TR-2004-027

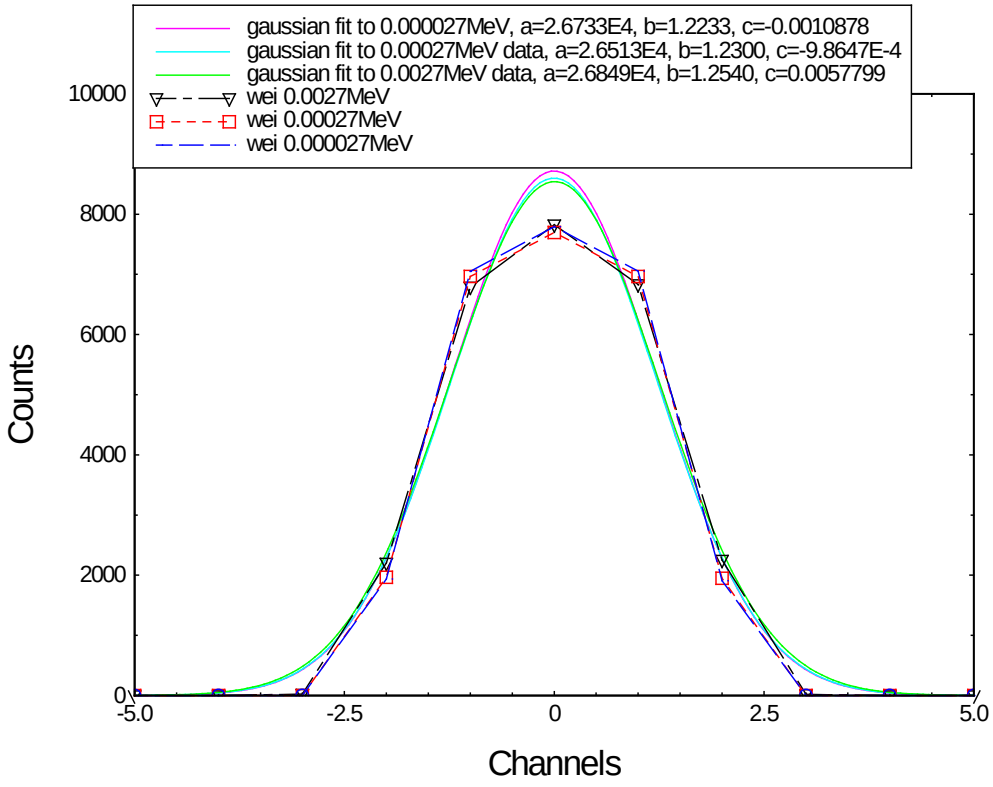

Figure 1: Event distributions comparing the three values of w_{ei} in the presence of electron diffusion with σ_o= 50μm/√cm and a drift distance of 65mm.

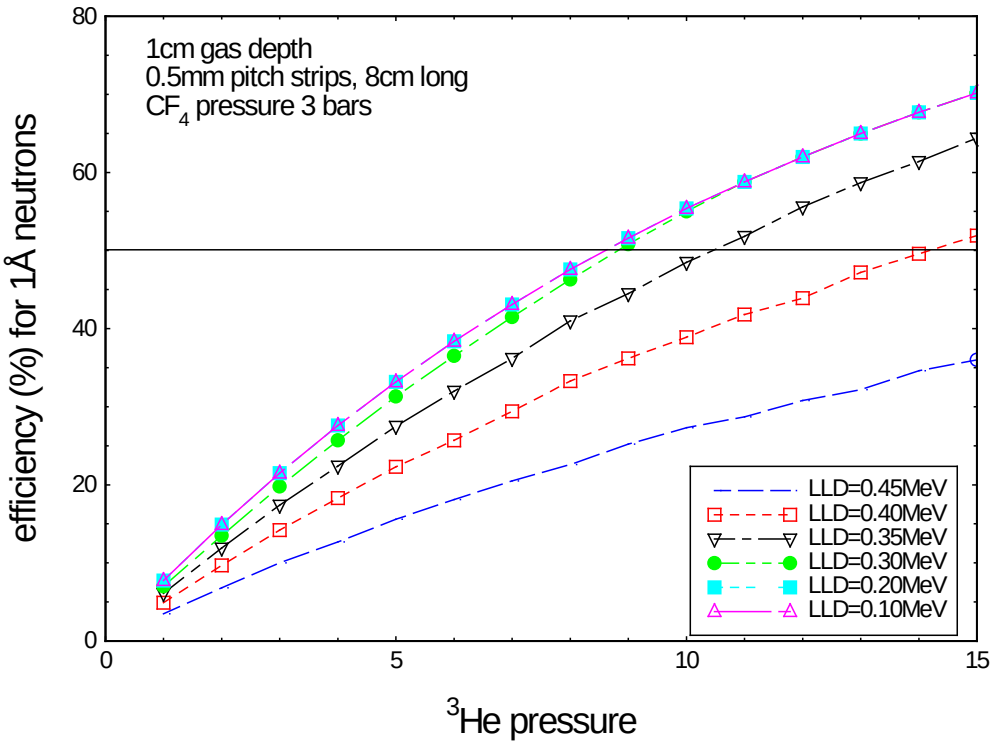

Figure 2: Variation of detection efficiency with ^{3}He pressure for 10mm of gas depth in a face-on geometry

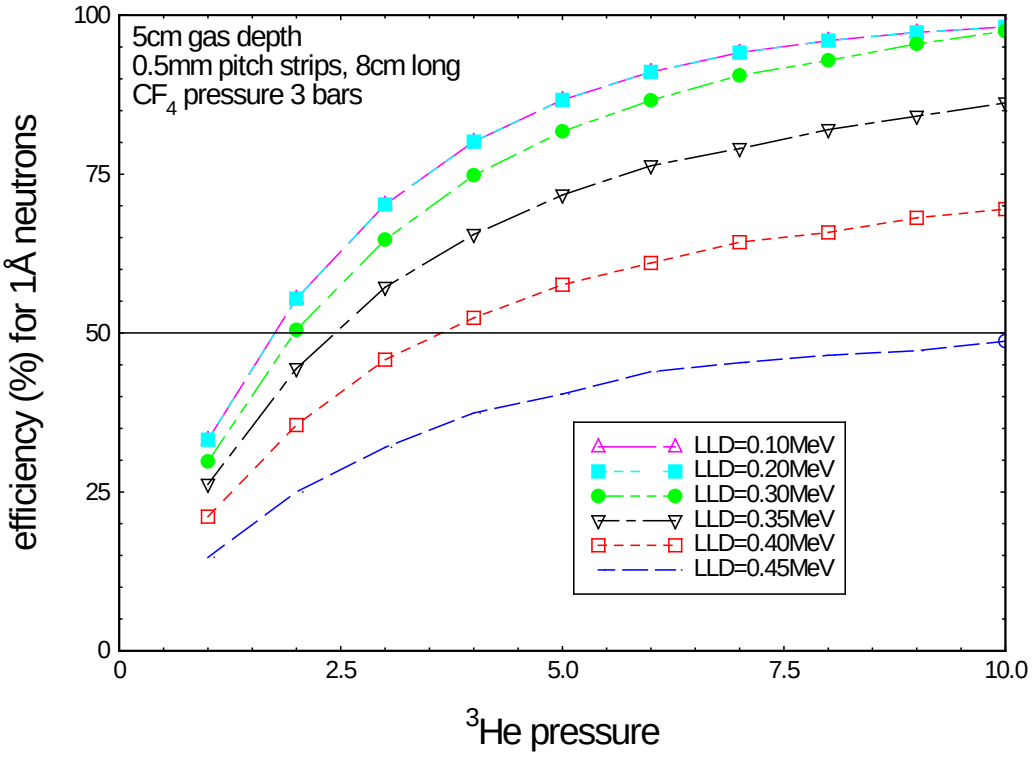

Figure 3: Variation of detection efficiency with ^{3}He pressure for 50mm of gas depth in a face-on geometry

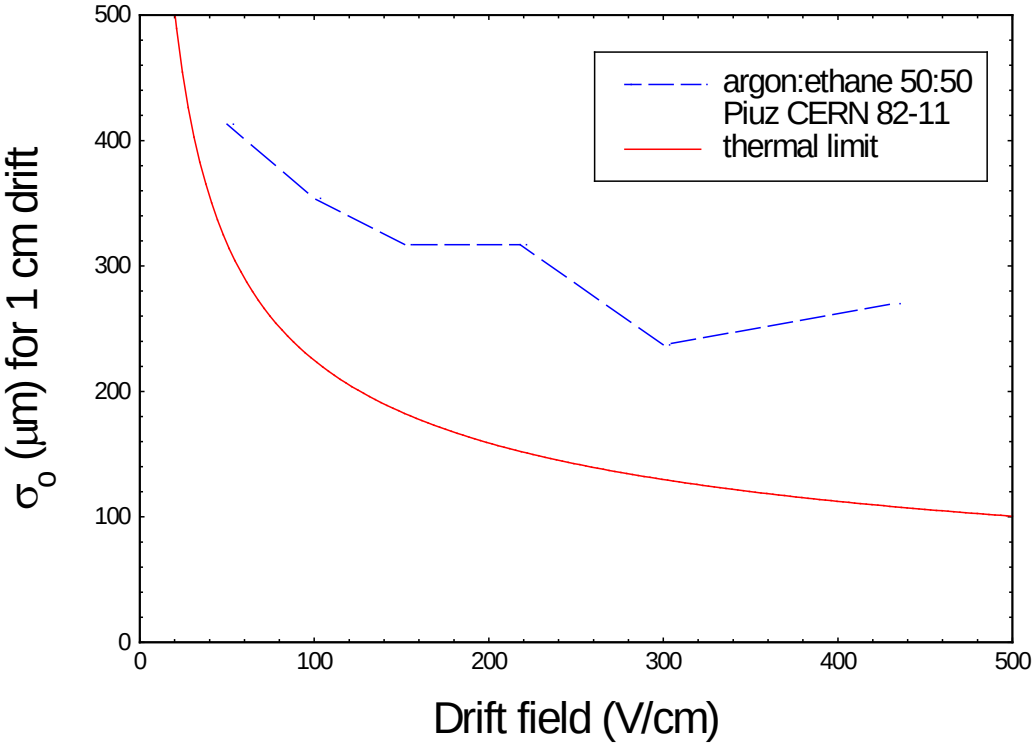

Figure 4: Plot of experimentally measured σ_o vs drift field showing the thermal limit, adapted from [14]

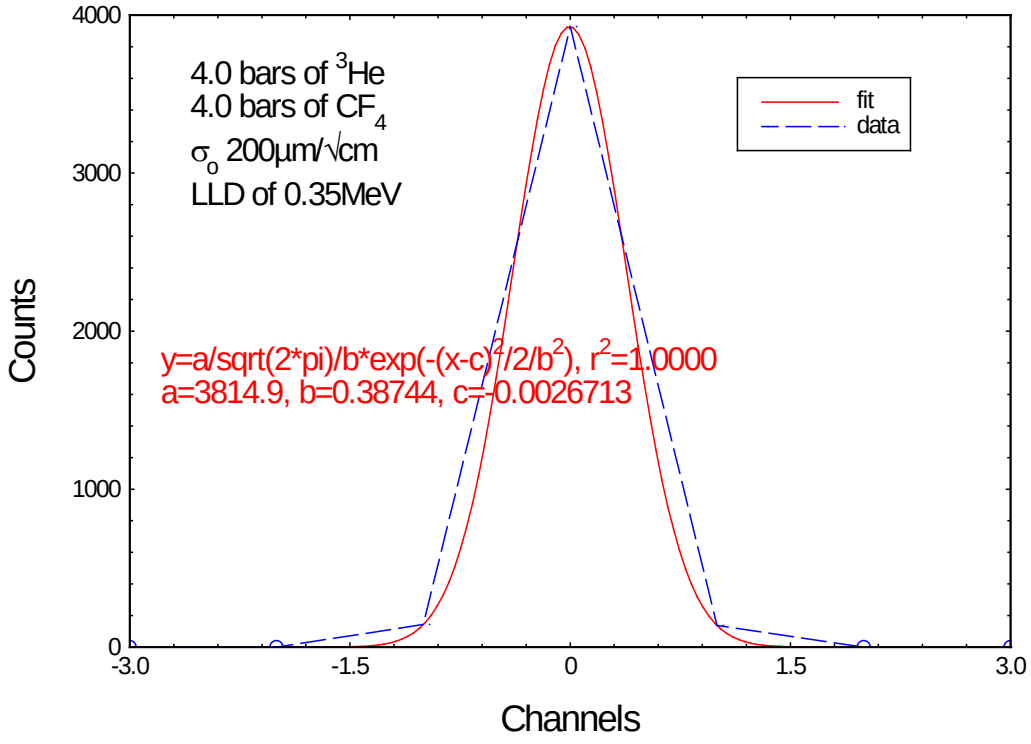

Figure 5: Event distribution for 4 bars of ^{3}He, 4 bars of CF_4, a σ_o of 200µm/√cm and an LLD of 0.35MeV for the pointing anode geometry

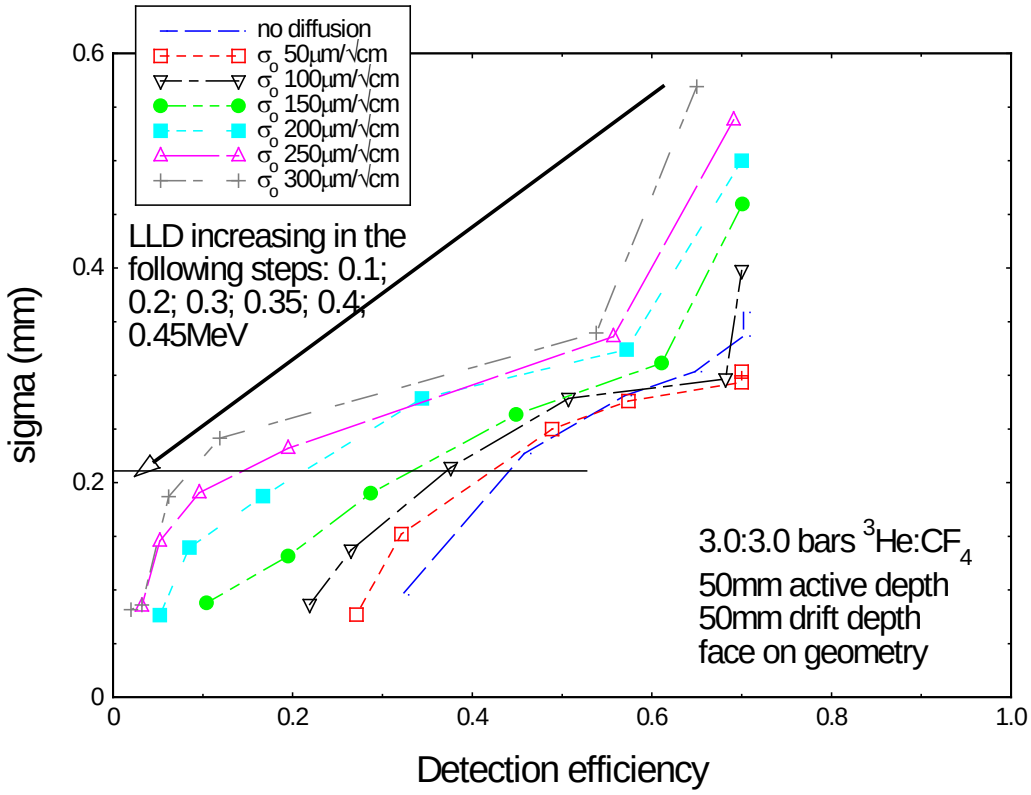

Figure 6: Variation of sigma as a function of detection efficiency for a 50mm gas depth, face-on geometry with 3.0 bars CF_4 and 3.0 bars of ^{3}He at various values of σ_o and LLD

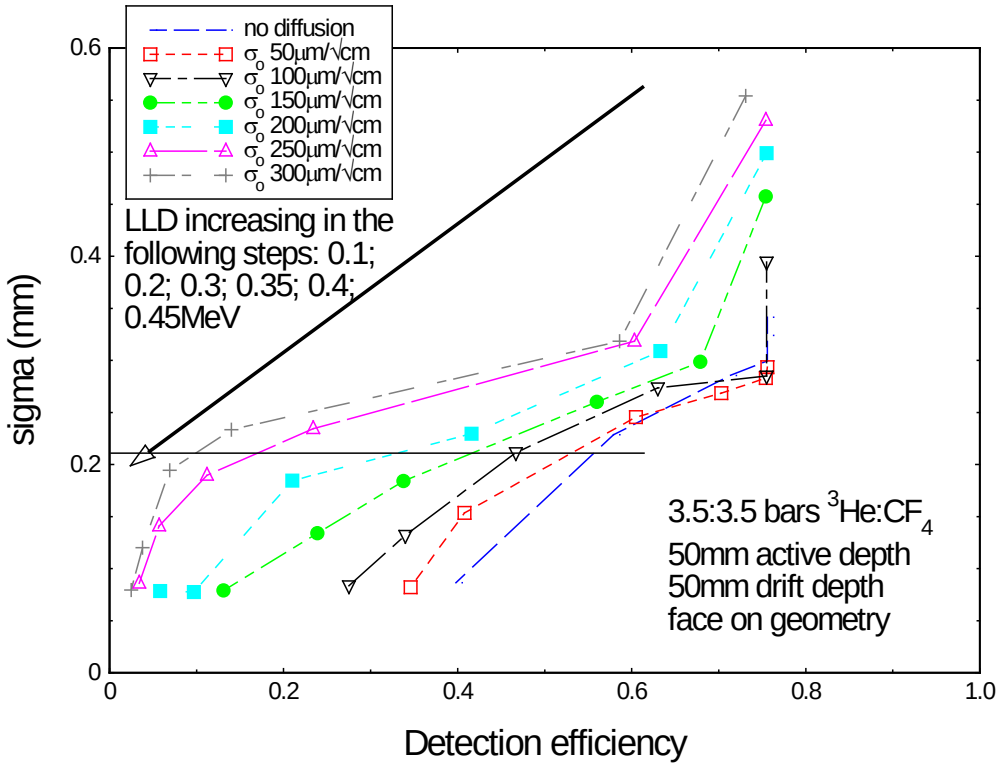

Figure 7:Variation of sigma as a function of detection efficiency for a 50mm gas depth, face-on geometry with 3.5 bars CF_4 and 3.5 bars of ^3He at various values of σ_o and LLD

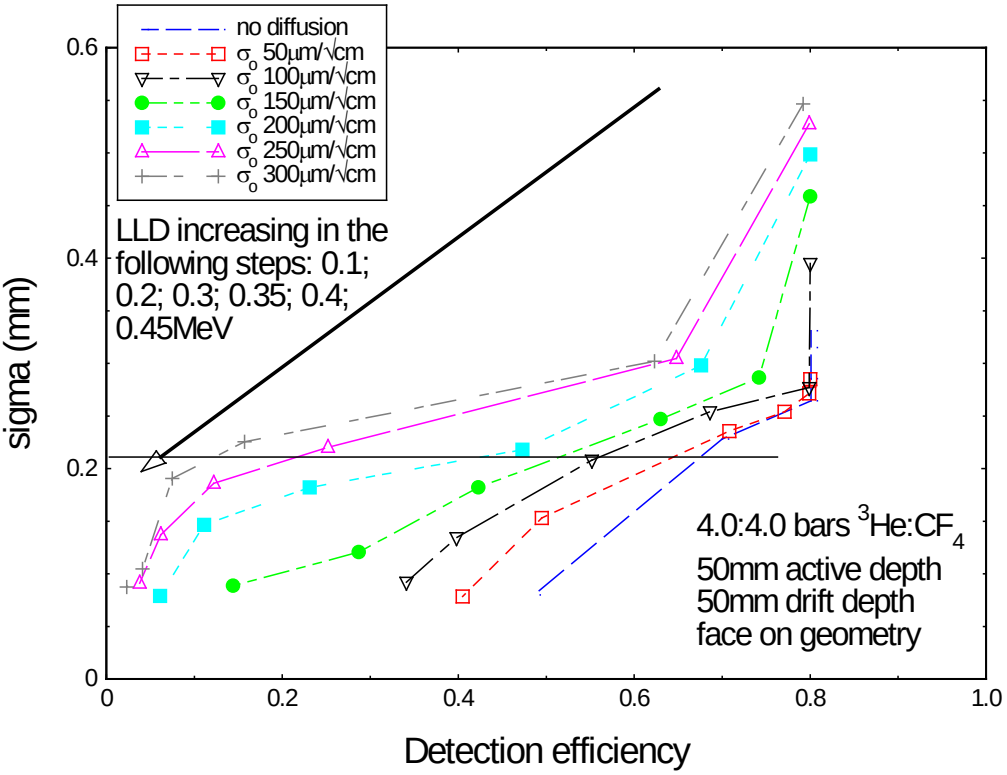

Figure 8: Variation of sigma as a function of detection efficiency for a 50mm gas depth, face-on geometry with 4.0 bars CF_4 and 4.0 bars of ^3He at various values of σ_o and LLD

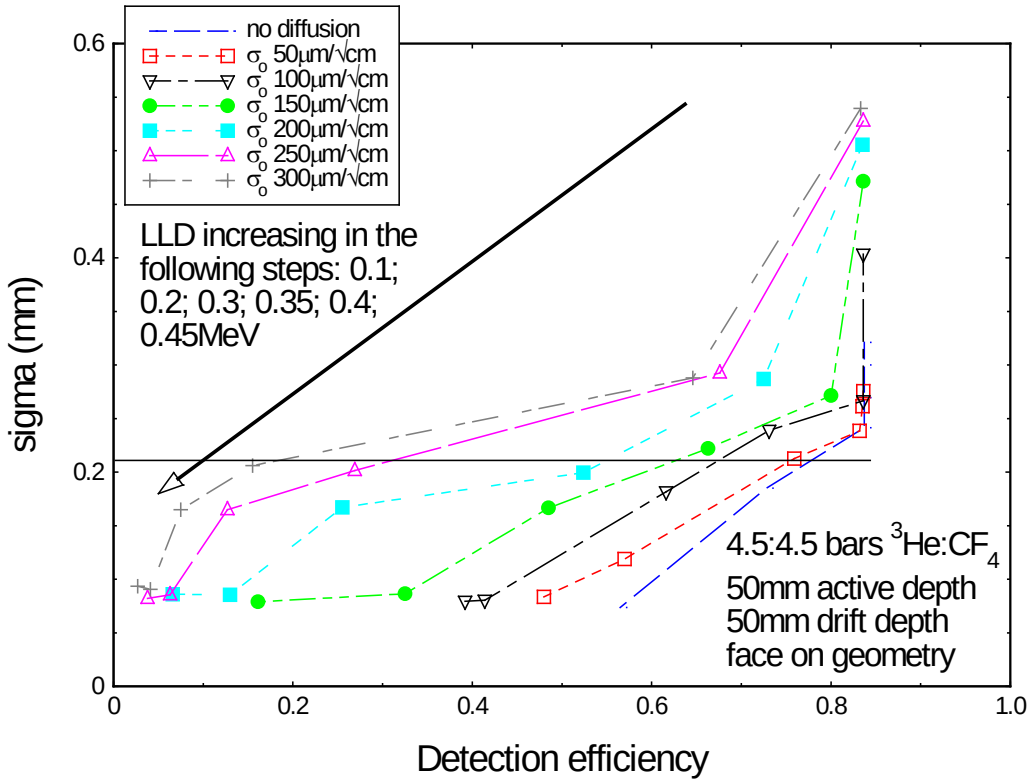

Figure 9: Variation of sigma as a function of detection efficiency for a 50mm gas depth, face-on geometry with 4.5 bars CF_4 and 4.5 bars of ^3He at various values of σ_o and LLD

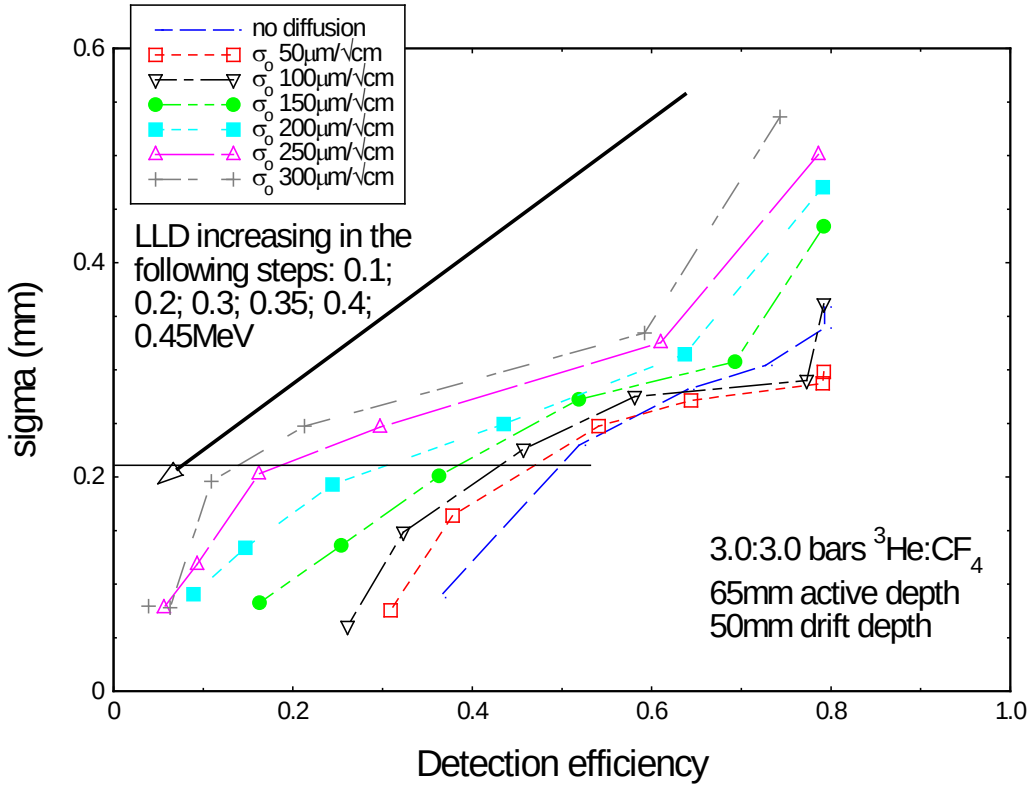

Figure 10: Variation of sigma as a function of detection efficiency for a 65mm gas depth, pointing-anode geometry with 3.0 bars CF_4 and 3.0 bars of ^3He at various values of σ_o and LLD

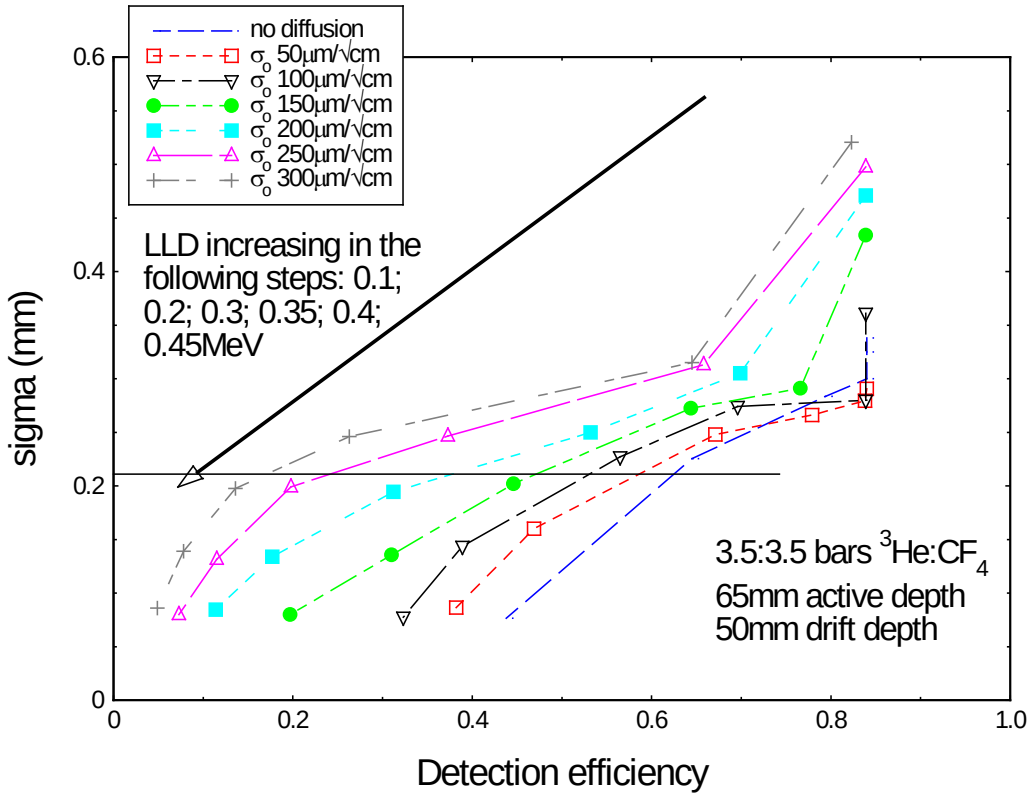

Figure 11: Variation of sigma as a function of detection efficiency for a 65mm gas depth, pointing-anode geometry with 3.5 bars CF_4 and 3.5 bars of ^3He at various values of σ_o and LLD

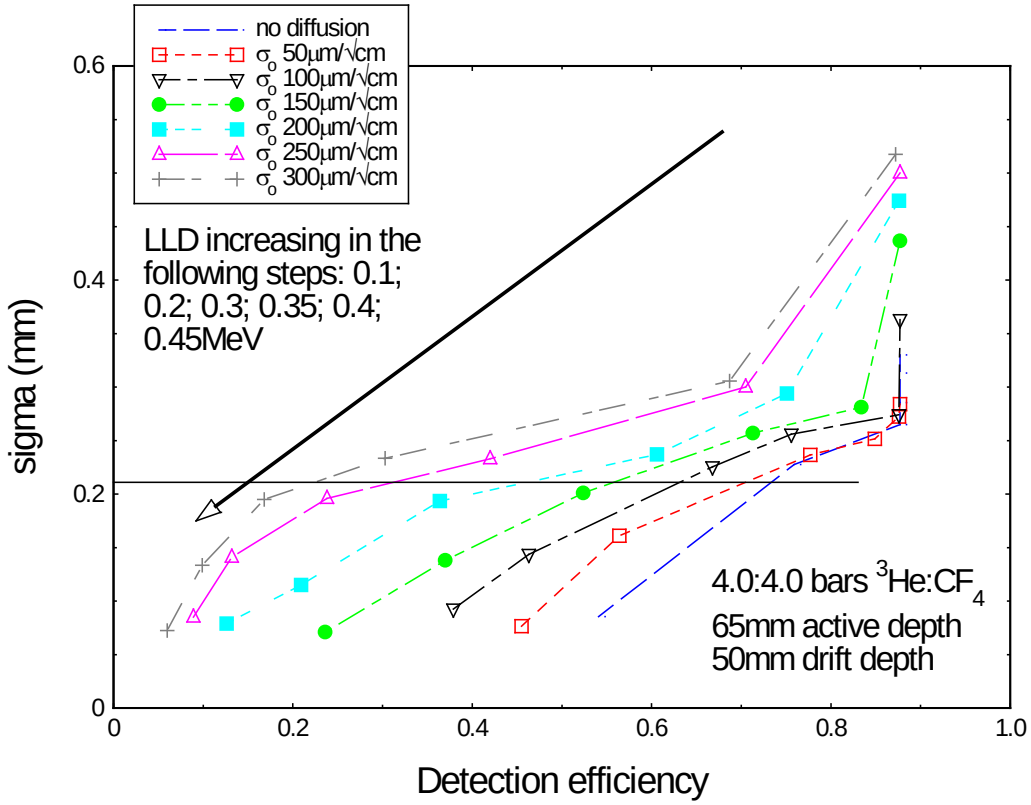

Figure 12: Variation of sigma as a function of detection efficiency for a 65mm gas depth, pointing-anode geometry with 4.0 bars CF_4 and 4.0 bars of ^3He at various values of σ_o and LLD

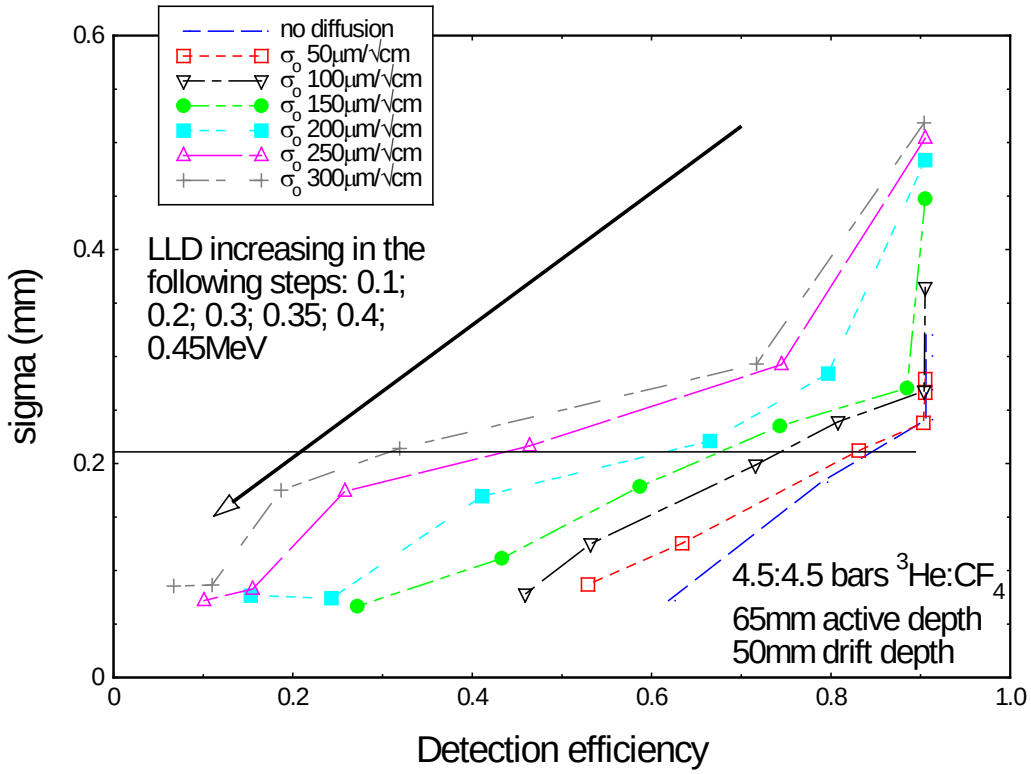

Figure 13: Variation of sigma as a function of detection efficiency for a 65mm gas depth, pointing-anode geometry with 4.5 bars CF_4 and 4.5 bars of ^3He at various values of σ_o and LLD

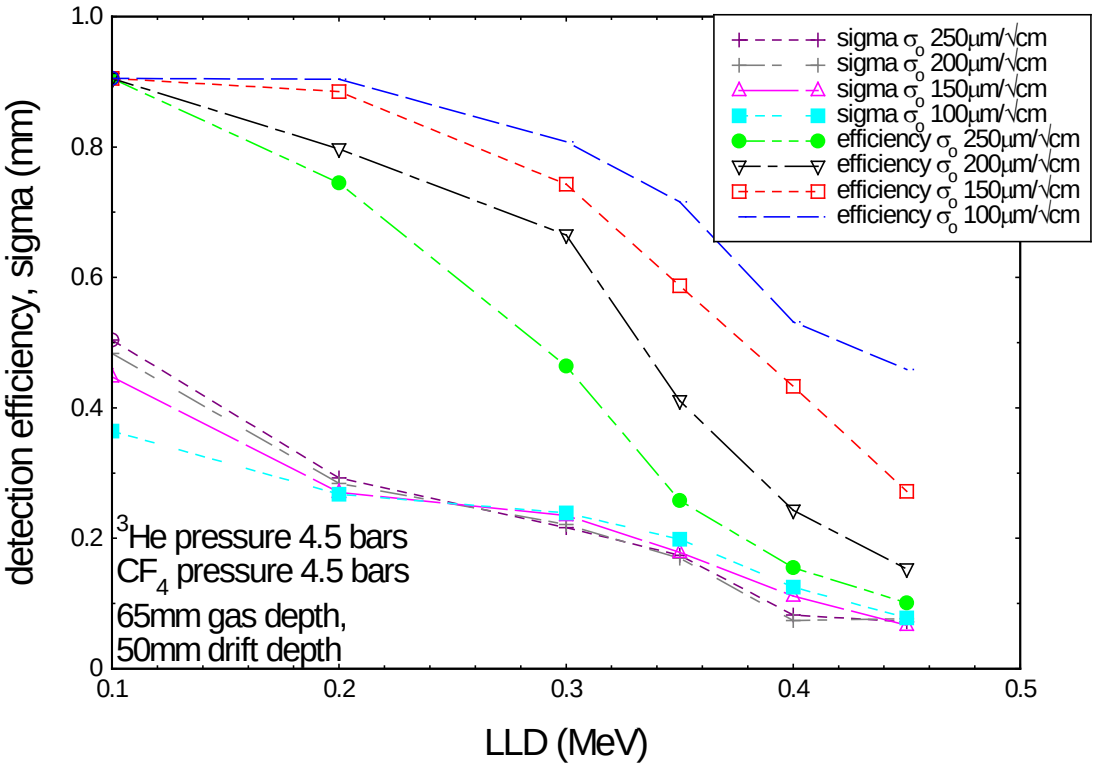

Figure 14: Variation of sigma and detection efficiency as a function of LLD for various values of σ_o with 4.5 bars CF_4 and 4.5 bars of ^3He for the pointing anode geometry

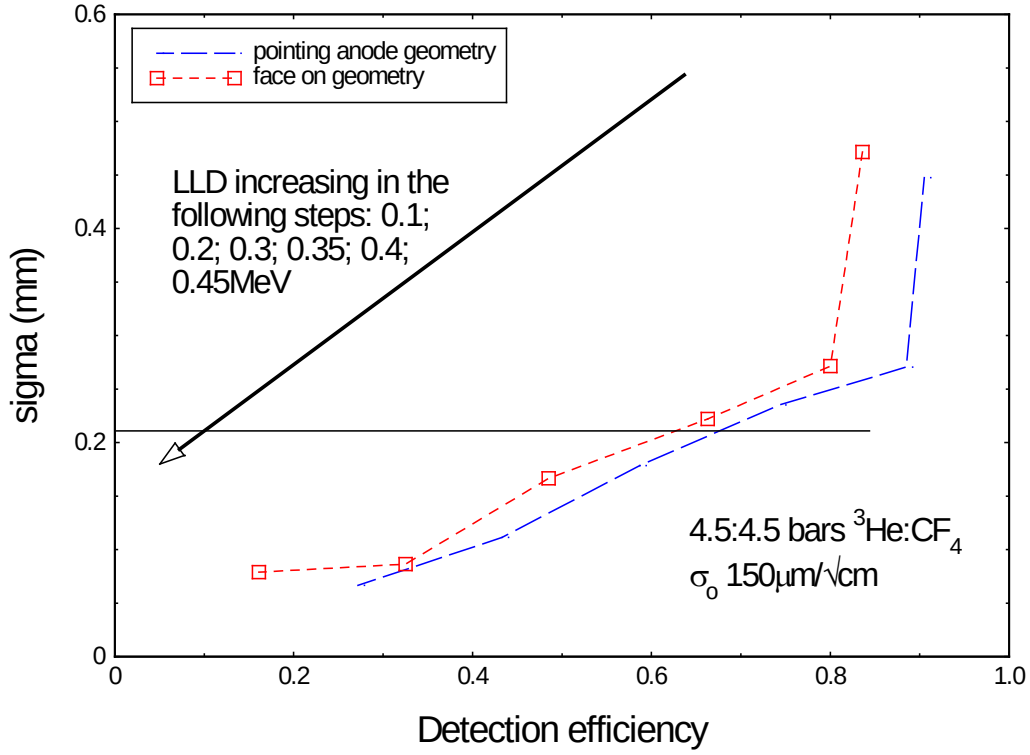

Figure 15: Direct comparison of sigma as a function of detection efficiency for both geometries with 4.5 bars CF_4 and 4.5 bars of ^{3}He

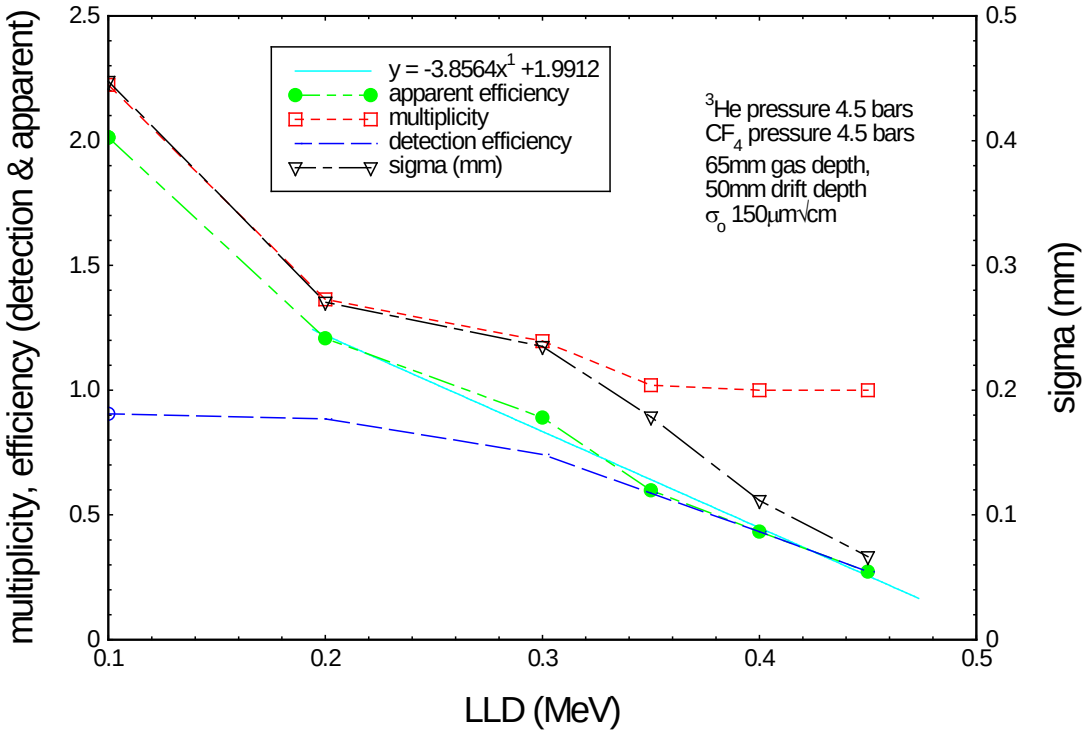

Figure 16: Variation of sigma, detection efficiency and multiplicity as a function of LLD with 4.5 bars CF_4 and 4.5 bars of ^{3}He for the pointing-anode case